

# Corrosion properties of oxygen plasma immersion ion implantation treated magnesium

G.J. Wan, M.F. Maitz, H. Sun, P.P. Li, N. Huang\*

Key Lab. of Advanced Technology for Materials of China Education Ministry, Sichuan Key Lab. of Surface Engineering of Artificial Organ, College of Materials Science and Engineering, Southwest Jiaotong University, Chengdu, 610031, China

Available online 19 April 2007

## Abstract

Oxygen plasma immersion ion implantation (PIII) was conducted in magnesium with oxygen doses in the range of  $2.5 \times 10^{15}$  ions  $\text{cm}^{-2}$  up to  $2.0 \times 10^{16}$  ions  $\text{cm}^{-2}$ , and the corrosion properties were investigated in neutral phosphate buffer solution (PBS, pH 7.4) and chloride ion enriched PBS (145 mM  $\text{Cl}^-$ , pH 6.4) (PBS( $\text{Cl}^-$ )). Significantly enhanced corrosion resistance against PBS was achieved on Mg treated with high oxygen doses above  $1 \times 10^{16}$  ions  $\text{cm}^{-2}$ . The corrosion current density  $I_{\text{corr}}$  of treated Mg was almost five orders less than that of untreated Mg; no intermediate values are obtained for samples with intermediate doses. However, all samples we prepared in this case could not withstand the more aggressive PBS ( $\text{Cl}^-$ ). No improvement of corrosion resistance in such solution has been observed even for surfaces implanted at  $2.0 \times 10^{16}$  ions  $\text{cm}^{-2}$ . The enhanced corrosion resistance against neutral PBS is ascribed to increased Mg–O bonding states formed on the surface layer of magnesium by the PIII process, as discerned by X-ray photoelectron spectroscopy (XPS) and X-ray diffraction (XRD) measurements. Further the more homogenous surface morphology, due to the ion bombardment effect, as observed by atomic force microscopy (AFM) may contribute. The Mg–O bondings can be dissolved easily in  $\text{Cl}^-$  enriched and more acidic ambience, as shown with PBS( $\text{Cl}^-$ ).

© 2007 Elsevier B.V. All rights reserved.

**Keywords:** Corrosion behavior; Surface modification; Plasma immersion ion implantation; Magnesium; Cardiovascular stents

## 1. Introduction

The attractive properties of magnesium as a notable lightweight structural metal offer great potential for technical applications such as in the automobile and aerospace fields [1], however poor corrosion resistance against many media often limits the widespread scope of applications [2,3]. Magnesium and its alloys were introduced into orthopaedic and trauma surgery in the first half of the last century [4], owing to the elastic modulus being closer to that of bone than most other metals as well as the *in vivo* degradability, by which a second operation for implant removal might be avoided. However, this approach was stopped, especially when the alternative stainless steel was successfully employed. The problem arises from uncontrollable degradation of magnesium *in vivo*, and in most circumstance the corrosion rates are too high. Furthermore, hydrogen-formation during the

corrosion process caused problems *in vivo*. Recently magnesium has intrigued scientists and technicians considering its use for vascular stent fabrication [5,6]. It is expected that that magnesium-stents can maintain a supporting function during the first weeks or months after implantation and after this time they degrade without risk of mechanical or chemical irritation causing restenosis. Modification or tailoring the corrosion resistance of Mg is therefore of great scientific and technical importance from this perspective.

In this study, we conduct oxygen plasma immersion ion implantation (PIII) into magnesium. This technique allows by its inherent non-line-of-sight capability to treat a complex geometry like biomedical implants [7]. The corrosion behavior was investigated in phosphate buffered solution (PBS) and chloride ion enriched PBS (145 mM  $\text{Cl}^-$  pH 6.4).

## 2. Experimental

1 mm thick magnesium sheets of 99.9% purity (Goodfellow, UK), were cut into discs 12 mm in diameter, then ground with

\* Corresponding author. Tel./fax: +86 28 87600625.

E-mail addresses: [nhuang@263.net](mailto:nhuang@263.net), [huangan@home.swjtu.edu.cn](mailto:huangan@home.swjtu.edu.cn) (N. Huang).

Table 1  
Instrumental conditions for oxygen PIII treatment for Mg

Samples	Target bias Voltage			RF power (W)	Oxygen working pressure (Pa)	Time (min.)	Oxygen implanted dose ( $\times 10^{15}$ ions $\text{cm}^{-2}$ )
	Voltage (KV)	Frequency (Hz)	Pulse width ( $\mu\text{s}$ )				
PIII-1						30	2.5
PIII-2	20	245	6.5	500	0.2	60	5
PIII-3						120	10
PIII-4						240	20

silicon carbide paper, and finally polished to a final roughness of approximately 0.02  $\mu\text{m}$ . After cleaning ultrasonically in acetone and ethanol, the samples were processed in our PIII instrument [8] at a base vacuum of  $1.2 \times 10^{-3}$  Pa. Before PIII, the surfaces were cleaned by argon sputtering (RF: 800W, DC Bias Voltage: 1000 V) to remove surface contaminations as well as some of the naturally grown surface oxide layer. Oxygen plasma was produced by a radio-frequency (r.f.) method, and immersion implantation was conducted by applying a pulsed bias voltage of  $-20$  kV to the target. Different oxygen implantation process doses can be anticipated by the following equation:

$$D = (NI_A t_p f T) / [(1 + \gamma) e A]$$

Where  $N$  is an ionizing factor;  $I_A$  the ion current;  $t_p$  the pulse width of the bias voltage;  $f$  the repetition frequency of the bias voltage;  $T$  the treatment time;  $\gamma$  an effect factor for secondary electrons;  $e$  the elementary electron charge;  $A$  the target surface area. The instrumental parameters are summarized in Table 1.

Surface chemical states of the modified Mg were determined by X-ray photoelectron spectroscopy (XPS, Model PHI 5600, Perkin-Elmer, USA) using monochromatic Mg Ka X-rays operating at 14 kV. The crystalline structure of the surface layer was determined by X-ray diffraction (XRD), and the spectra were recorded in grazing angle method (GAXRD) at an angle of incidence  $\omega = 0.5^\circ$  (X'Pert Pro MPD, Philips, Netherlands). The surface topography of the samples was analyzed by atomic force microscopy in tapping mode (AFM, SPI 3800N, SEIKO).

Potentiodynamic polarization tests were executed on an IM6 electrochemical workstation (Zahner, Germany) in the two types of electrolyte, PBS and  $\text{PBS}(\text{Cl}^-)$  respectively (composition in Table 2). A standard three electrode set-up was applied where a platinum slice was used as counter electrode, a saturated calomel electrode (SCE) with Luggin bridge arrangement as reference electrode, and the samples were epoxy-sealed to expose only a defined investigation surface as working

Table 2  
Composition for two corrosion testing electrolytes

Solution	$\text{Na}_2\text{HPO}_4$ (g/L)	$\text{KH}_2\text{PO}_4$ (g/L)	$\text{NaCl}$ (g/L)	$\text{KCl}$ (g/L)	$\text{HCl}$ (mM)	pH
PBS	11.928	2.176	–	–	–	7.4
$\text{PBS}(\text{Cl}^-)$	11.928	2.176	8.0	0.2	5 mM	6.4

Note: approximately 5 mM additional HCl was used to adjust the pH value of  $\text{PBS}(\text{Cl}^-)$  to 6.4.

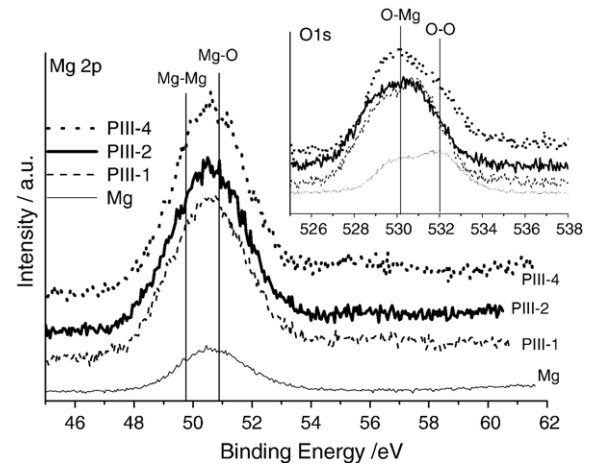


Fig. 1. Mg 2p and O 1s core level XPS spectra of untreated Mg and oxygen PIII processed Mg.

electrodes. Before recording current/potential ( $I/E$ ) curves, each sample was kept in the testing solution for 20 min at open circuit potential (OCP) to reach a relatively stable condition. Polarization curves were obtained by scanning from 200 mV more negative than the OCP to 0.5 V/SCE at a rate of 2 mV/s. Scanning electron microscopy (SEM, Quanta200, FEI) observation and energy dispersive X-ray (EDX) analysis were performed together to examine the surface characteristics after potentiodynamic polarization corrosion.

### 3. Results and discussions

Fig. 1 shows the surface photoelectron peaks of Mg 2p and O 1s acquired from the four samples. The spectrum was calibrated using the Ar 2p peak at 241.9 eV according to the handbook

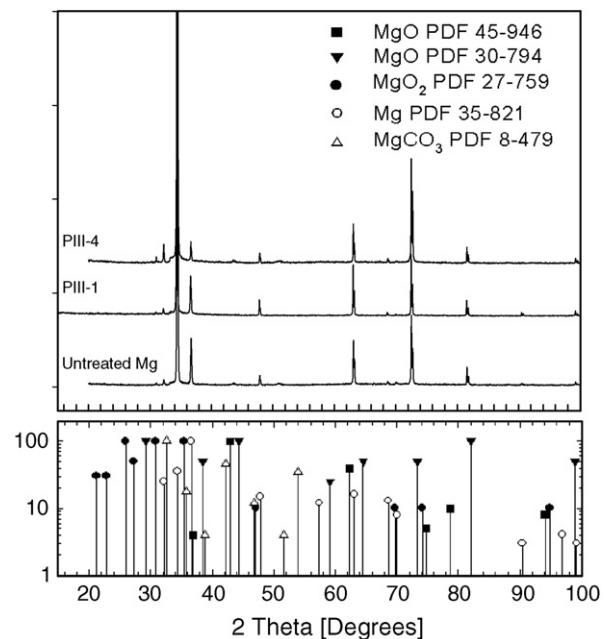


Fig. 2. Surface layer XRD pattern of untreated magnesium and samples PIII-1 and PIII-4.

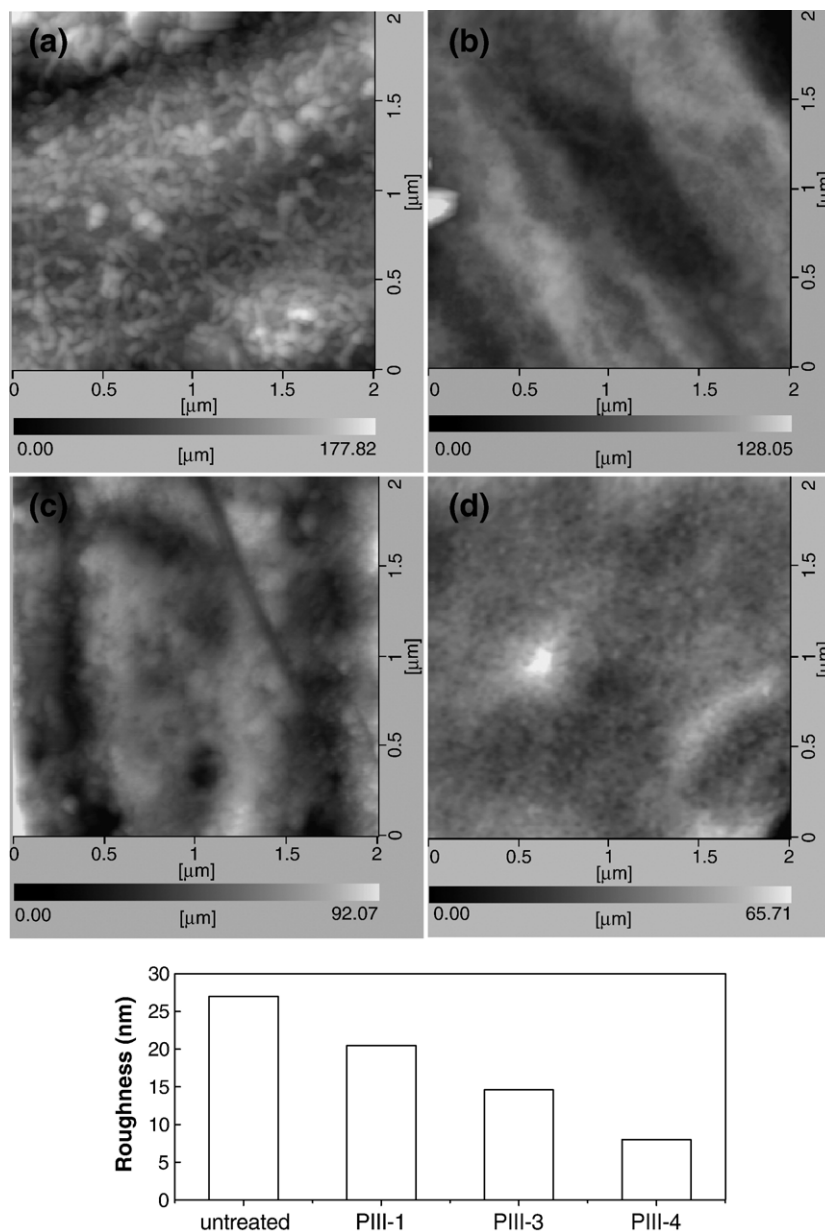


Fig. 3. Top: Surface morphology AFM images of untreated Mg (a) and oxygen PIII treated Mg samples: (b) PIII-1; (c) PIII-3; (d) PIII-4. Bottom: RMS surface roughness values of the samples, obtained on representative  $2 \times 2 \mu\text{m}^2$  scans.

published by Physical Electronics (PHI) [9]. In all cases the Mg 2p peak can be deconvoluted into two main components, one at 50.8 eV indicative of Mg–O and another at a lower energy attributable to Mg–Mg at 49.7 eV [9,10]. A tendency to higher energy can be seen on samples with increased oxygen doses implanted, indicating an increased number of Mg–O bonds due to the oxygen PIII process. The O1s peaks of the samples also can be deconvoluted into two components of O–O bonds at 532 eV and Mg–O bonds at 531.0 eV [9,11]. The low energy shoulder of Mg–O as well as shifts of the peak to lower energies consistently emerge when the oxygen implantation dose increases. These findings strongly corroborate the formation of Mg–O bondings by oxygen ion implantation. It must be noted that some absorbed or residual molecular oxygen from the vacuum in the XPS chamber, as well as preformed oxidation

on the as-sputtered Mg surface, may influence the anticipated O/Mg ratio. This is a common problem for such extremely reactive metals, and no further effort has been made to determine the exact bonding contributions. The observed binding energy shifts clearly prove that increased Mg–O binding states are achieved by higher oxygen implantation doses.

For analysis of the phase structure of the modified layer, XRD spectra were taken (Fig. 2). Although an incident angle as low as  $0.5^\circ$  was used, the pattern is dominated by bulk magnesium. The high contribution of the bulk is seen in the low implantation depth of about 119 nm for oxygen in magnesium at  $-20$  kV bias voltage (SRIM calculation, SRIM.com (USA) and Hahn-Meitner Inst. (Germany)) and the relatively low implantation doses in this study. Characteristic oxide peaks appeared at  $36.9^\circ$ ,  $73^\circ$  and  $81.5^\circ$ , both on untreated and treated samples

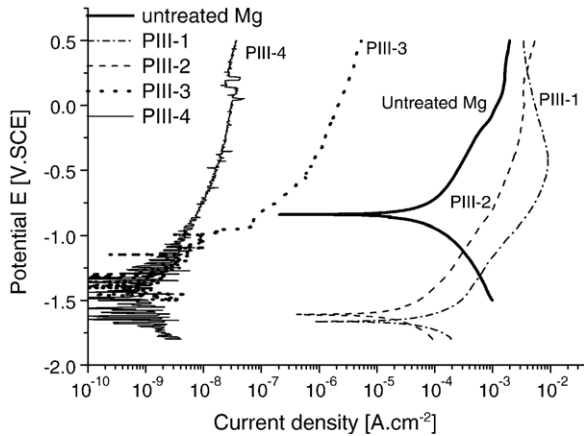


Fig. 4. Potentiodynamic polarization curves of untreated Mg and oxygen PIII treated Mg in PBS.

[12]. This indicates a relatively thin oxide layer as well as comparatively low oxygen implantation doses.

Ion implantation changes the surface topography, which has impact also on the corrosion properties of the metal. AFM images of the untreated Mg reveal a very porous albeit fine crystalline surface (Fig. 3). After PIII treatment, all sample surfaces appear more homogenous. The surface of the low dose implanted sample of PIII-1 has some irregular clusters on the surface, and at higher magnification many pit-like defects appear. The samples of PIII-3 and PIII-4 have much more homogeneous and smoother surfaces, and the latter surface appears most homogeneous. The uniform surface characteristic can be attributed both to the sputtering effects of incident ion bombardment and to diffusion processes due to the energy impact of PIII process. A homogeneous, smooth surface

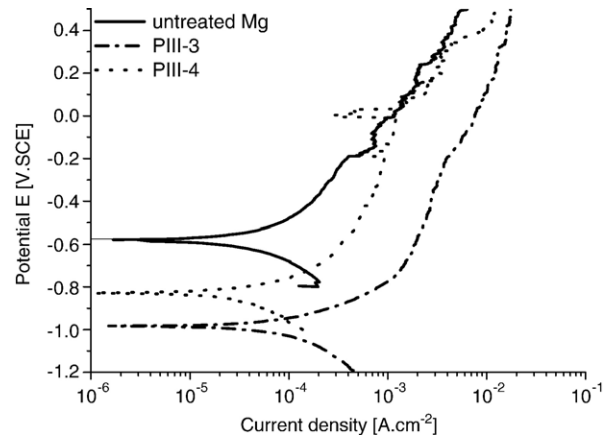


Fig. 6. Potentiodynamic polarization curves of untreated Mg, selected oxygen PIII treated Mg in PBS(Cl<sup>-</sup>).

certainly has better corrosion properties, as there is less additional surface due to roughness and fewer nuclei to initiate pitting corrosion.

Fig. 4 shows potentiodynamic  $I/E$  curves of oxygen ion implanted Mg at different doses in PBS with a control sample of untreated Mg for comparison. In all cases, oxygen ion implantation caused an up to 1 V more negative corrosion potential than the untreated Mg. This is another indication that surface oxides formed by the unbalanced method of PIII differ from the natural surface oxidation. From a thermodynamic point of view, one would expect the more negative corrosion potential of the ion implanted samples to lead to lower stability. However, the corrosion current density  $I_{\text{corr}}$  decreased strongly by almost five orders of magnitude for samples PIII-3 and PIII-4. Implantation at lower doses did not influence the corrosion

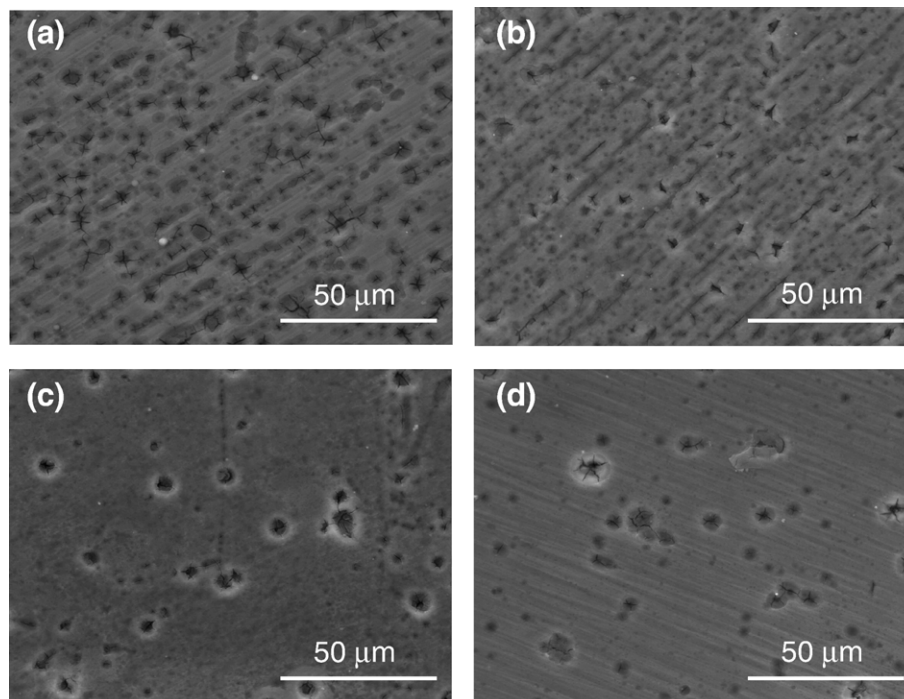


Fig. 5. Surface SEM images of untreated Mg, oxygen PIII treated Mg after polarization corrosion in PBS (a) untreated Mg; (b) PIII-1; (c) PIII-3; (d) PIII-4.

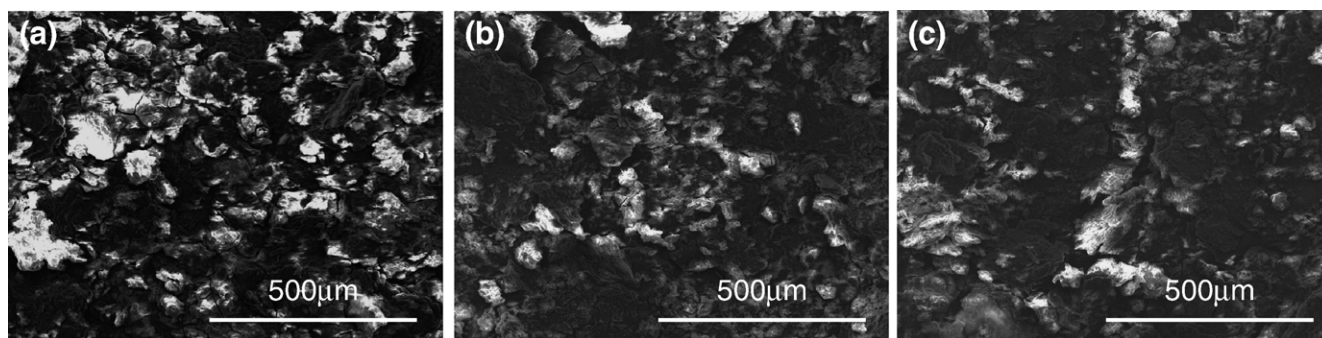


Fig. 7. Surface SEM images of untreated Mg, oxygen PIII treated Mg after polarization corrosion in PBS ( $\text{Cl}^-$ ): (a) untreated Mg; (b) PIII-3; (c) PIII-4.

current density; intermediate corrosion rates for intermediate implantation dose could not be achieved. This indicates that oxygen ion implantation on Mg significantly improves the corrosion resistance against PBS and that there exists a threshold value of implantation dose to obtain this modification.

The SEM surface characteristics of the samples after 0.5 V/SCE anodic polarization scanning are shown in Fig. 5. The predominant type of corrosion for all samples is pitting corrosion. However the maximum pitting depth and diameter vary with oxygen implantation dose. The corroded surface of native magnesium had a great amount of pits with big size and high depth, and deep cracks are also observed at some sites as an indication of intergranular corrosion. Beyond that, corrosion also readily occurs at susceptible sites such as along the polishing grooves. The surfaces of untreated magnesium and PIII-1 after the corrosion test in PBS look similar in SEM; there were only slightly less pits formed on PIII-1. A different appearance was observed for samples PIII-3 and PIII-4, which have significantly less and mainly superficial pitting. On samples PIII-4 also the polishing lines were less attacked by corrosion, demonstrating the protective properties of the oxide layer.

We attribute the enhanced corrosion resistance of the long time treated samples against PBS to increased Mg–O bonding states, higher thickness of the oxide layer, as well as the more homogenous surface properties achieved by the oxygen PIII process. Phosphate ions and water can readily oxidize or hydroxidize the elemental Mg, but they hardly react with magnesium oxides [13]. Further, the more homogeneous surface obtained by ion bombardment reduces the risk of pitting corrosion, as it has more uniform energy states. Heat accumulation during the ion implantation process may lead to deeper diffusion of oxygen ions, higher film thickness and more complete oxidation of magnesium. The target temperature of PIII-4 can reach approximately  $200^\circ\text{C}$  during the PIII process, while sample PIII-1 can only reach  $120^\circ\text{C}$ .

We investigated further corrosion performance of the modified Mg in chloride enriched PBS ( $145\text{ mM Cl}^-$ , pH 6.4), which is more similar to biological fluids [14]. It is well known that magnesium is highly susceptible to corrosion even at low chloride concentrations ( $2\text{ mM}$ ) or decreased pH [15]. Also in this study, no improved corrosion resistance in  $\text{Cl}^-$  enriched PBS was observed for any of the ion implanted Mg samples compared to the untreated magnesium (Fig. 6)  $\text{Cl}^-$  at lower pH easily dissolved the Mg–O phase, and the pits formed did not oxidize and repair per se [16,17]. Cracking by intergranular corrosion

could still be observed in SEM. Corrosion in this medium leads to the formation of corrosion products that cover the surface in a non-protective way. They do not dissolve in water and are hard to remove even by ultrasound (Fig. 7) This is inappropriate for most medical applications. Composition and biocompatibility are not completely investigated. According to EDX spectra, the products consist of magnesium chloride and more complex compounds. The corrosion performance of magnesium and magnesium oxides in buffers with more physiological composition as well as tailored corrosion rates in simulated body fluid needs further investigation.

#### 4. Conclusions

Magnesium was treated by oxygen plasma immersion ion implantation. Increased Mg–O bond states were achieved by increasing the oxygen dose and substrate temperature at longer treatment time. Such oxide-rich layers offer significant corrosion protection against a phosphate buffer. Nevertheless, even the samples with highest treatment doses in our case could not withstand  $145\text{ mM Cl}^-$  containing and acidified PBS. Hardly controllable corrosion rates in chloride ion containing solutions, such as body fluid, may still be the biggest problem for biomedical applications of magnesium. Further work needs to be focused on this subject to solve the stringent problem [2,18].

#### Acknowledgements

This research was jointly supported financially by Boston Scientific SCIMED (USA), the Natural Science Foundation of China (30318006, 30670565, 20603027), and the Key Basic Research Program 2005CB623904.

#### References

- [1] J.E. Grayand, B. Luan, *J. Alloys Compd.* 336 (2002) 88.
- [2] C.L. Makar, J. Kruger, *Int. Mater. Rev.* 38 (1993) 138.
- [3] Guangling Song, Andrej Atrens, David H. Stjohn, Xianliang Wu, Jason Nairn, *Corros. Sci.* 39 (10–11) (1997) 1981.
- [4] F. Witte, V. Kaese, H. Haferkamp, E. Switzer, A. Meyer-Lindenberg, C.J. Wirth, H. Windhagen, *Biomaterials* 26 (2005) 3557.
- [5] B. Heublein, R. Rohde, V. Kaese, M. Niemeyer, W. Hartung, A. Haverich, *Heart* 89 (2003) 651.
- [6] C. Di Mario, H. Griffiths, O. Goktekin, N. Peeters, J. Verbist, M. Bosiers, K. Deloosse, B. Heublein, R. Rohde, V. Kasese, C. Ilsley, R. Erbel, *J. Interv. Cardiol.* 17 (2004) 391.

- [7] P.K. Chu, S. Qin, C. Chan, N.W. Cheung, L.A. Larson, *Mater. Sci. Eng. Reports* 17 (1996) 207.
- [8] G.J. Wan, N. Huang, Y.X. Leng, P. Yang, J.Y. Chen, J. Wang, H. Sun, *Surf. Coat. Technol.* 186 (2004) 136.
- [9] J.F. Moulder, W.F. Stickle, P.E. Sobol, K.D. Bomben, *Handbook of X-ray Photoelectron Spectroscopy*, Perkin-Elmer, 1992.
- [10] D.R. Jennison, P. Weightman, P. Hannah, M. Davies, *J. Phys. C.* 17 (1984) 3701.
- [11] S. Verdier, N. van der Laak, S. Delalande, J. Metson, F. Dalard, *Appl. Surf. Sci.* 235 (2004) 513.
- [12] P.O. Ghelkier, S. Mahieu, G. De Winter, R. De Gryse, D. Depla, O.I. Lebedev, *Solid State Phenom.* 105 (2005) 433.
- [13] F. Stippich, E. Vera, G.K. Wolf, G. Berg, C. Friedrich, *Surf. Coat. Technol.* 103–104 (1998) 29.
- [14] L. Li, J. Gao, Y. Wang, *Surf. Coat. Technol.* 185 (2004) 92.
- [15] A. Antonyraj, C.O. Augustin, *Bull. Electrochem.* 15 (3–4) (1999) 135.
- [16] G. Song, A. Atrens, D. St John, X. Wu, J. Nairn, *Corros. Sci.* 39 (10–11) (1997) 1981.
- [17] G. Song, A. Atrens, X. Wu, B. Zhang, *Corros. Sci.* 40 (1998) 1769.
- [18] A.L. Rudd, C.B. Breslin, F. Mansfeld, *Corros. Sci.* 42 (2000) 275.